Gondwana Research 37 (2016) 172–181

Contents lists available at ScienceDirect

Gondwana Research

journal homepage: www.elsevier.com/locate/gr

GR Letter

Resolving the paradigm of the late Paleozoic–Triassic Chilean magmatism: Isotopic approach

A. del Rey [a,*], K. Deckart [a,b], C. Arriagada [a], F. Martínez [a]

[a] Departamento de Geología, Universidad de Chile, Santiago, Chile
[b] Advanced Mining Technology Centre (AMTC), Universidad de Chile, Santiago, Chile

ARTICLE INFO

Article history:
Received 18 December 2015
Received in revised form 6 May 2016
Accepted 6 June 2016
Available online 16 July 2016

Handling Editor: J.G. Meert

Keywords:
Pangea assemblage
U–Pb geochronology
O–Hf isotopes
Zircon
Andean orogenic cycle

ABSTRACT

The Andean orogenic cycle and its subduction-related magmatism along the southwestern margin of South America began during the early Jurassic after an accretionary history throughout Paleozoic times. The Chilean and Argentinian Frontal Andes batholiths, together with the Coastal Batholith, represent most of the pre-Andean orogenic cycle plutonism. However, how late Paleozoic–Triassic magmatism occurred along this margin and its transition to the Andean orogenic cycle still remains unclear. Here we present a geodynamic model using all the available published Lu–Hf and oxygen isotopic data ranging from latitudes 28° to 40°S, together with 5 new Hf–O data and U–Pb zircon ages from the Chilean Frontal Andes. Data indicate that subduction began at least in the latest early Carboniferous and was continuous throughout the late Paleozoic–Triassic period. Isotopic and geochronological results show a continuous magmatic trend, from high $\delta^{18}O$ values (continental) to mantle-like signatures, as the rocks get younger. Between latest early Carboniferous and earliest middle Permian, magmas formed in a subduction-related arc during the Gondwanide Orogeny. Later, throughout middle Permian to Triassic, magmatism occurred in a slab rollback extensional setting, triggered by low subducting plate velocities while Pangea was essentially in a static reference mode. There is no evidence for cessation of subduction during the Triassic and its renovation in the early Jurassic as previous work suggested. Therefore, we propose that Andean subduction has been a continuous tectonic process since Paleozoic times, whose initial geodynamic evolution was directly related to the Gondwanide Orogeny as part of the Pangea Assembly. Slab rollback, as well as shallowing and steepening of the subduction angle were among the triggers for the change in the type of magmatism observed among these rocks.

1. Introduction

Although it is one of the Earth's main plate boundaries, a complete comprehensive tectonic model for the paleo-South American southwestern margin in Chile does not exist. Specifically, the late Paleozoic–Triassic magmatism in Chile still has several important issues that remain unaddressed. First of all, how are these rocks related genetically along the Chilean margin (particularly from 28° to 40°S)? Second – and most important – in what tectonic setting did they originate? Traditionally, the geodynamic evolution has been explained through a collisional model (Ramos, 1988), which indicates that the southwestern part of South America registered a tectonic history dominated by the progressive accretion of allochthonous and/or para-autochthonous terranes. According to that model, the last stage of the Paleozoic collision involves the amalgamation of the Chilenia terrane at the western margin of Gondwana during Devonian times (Ramos et al., 1986; Álvarez et al., 2011) and the Patagonia terrane at the southwestern margin in the early Permian (Ramos, 2008). The eastward subduction of the paleo-Pacific oceanic plate under the Chilenia continental basement was responsible for the latest early Carboniferous–early Permian calc-alkaline I-type magmatism, now observed in the north-central Chilean and Argentinian Frontal Andes. Subsequently, during the Permian–Triassic period, calc-alkaline to transitional A-type granites were related to rifting (Mpodozis and Kay, 1992), which is associated with the Choiyoi province (23°S to 42°S in Chile and Argentina (Kay et al., 1989; Kleiman and Japas, 2009)). Based on these ideas, the change in the tectonic setting and thus its magmatism, has been interpreted as a consequence of a cessation in subduction after the accretion of an exotic, unidentified, 'terrane X' on the western side of Chilenia during the middle Permian (Mpodozis and Kay, 1992). This hypothetic collision was responsible for the cessation of subduction and therefore, formed the trigger for rifting conditions (extension due to slab collapse and lithospheric delamination). Re-establishment of subduction along the Chilean margin in the earliest Jurassic marked the initiation of the Andean orogenic cycle, which has continued without interruption to the present day (e.g. in Patagonia (Hervé et al., 2007)).

* Corresponding author.
E-mail address: alvherna@ing.uchile.cl (A. del Rey).

http://dx.doi.org/10.1016/j.gr.2016.06.008
1342-937X/

However, the tectonic process controlling the magmatism linking the Paleozoic accretionary history and the Jurassic Andean orogenic cycle is not clearly understood. Complete absence of geological evidence for the 'terrane X' and the remaining question whether subduction was renewed or intensified at the beginning of the Jurassic (Charrier et al., 2014) make the late Paleozoic–Triassic Chilean magmatism a crucial source of evidence. Moreover, there is no previous work relating all the intrusive units from that period of time (at least from 28° to 40°S). On the contrary, it has been suggested that units north and south of 33°S are genetically unrelated (Charrier et al., 2014; Hervé et al., 2014), arguing that the emplacement ages differ considerably between southern and northern plutons. Here we use all the available published Lu–Hf and oxygen isotopic data ranging from latitudes 28° to 40°S, together with 5 new Hf–O data and U–Pb zircon ages from the Montosa–El Potro Batholith (28°–28°30′S) in the Chilean Frontal Andes (Fig. 1) to propose a new tectonic scenario, and thus challenge previous models by

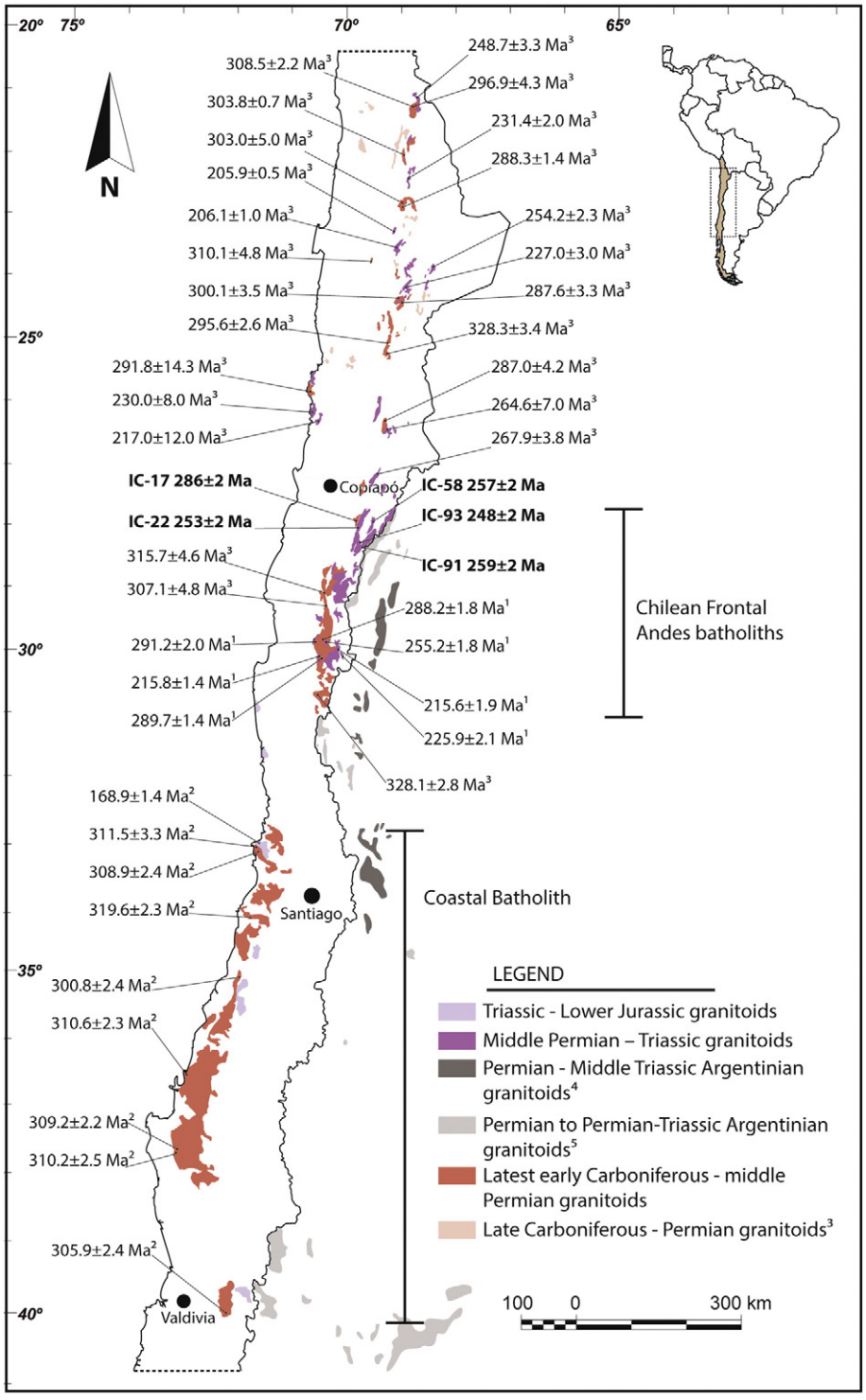

Fig. 1. Geographical distribution of the Chilean Frontal Andes late Paleozoic–Triassic batholiths and the Coastal Batholith (from ca. 20°S to 40°S). The location of the samples and their U–Pb crystallization ages are indicated (IC-17, IC-22, IC-58, IC-91, IC-93, this work; 1, Hervé et al. (2014); 2, Deckart et al. (2014); 3, Maksaev et al. (2014)). Tera Wasserburg concordia and age probability density plots of the analyzed samples are given in Fig. 2. Sample groups 1 and 2 have Hf–O isotopic data associated with the U–Pb ages (Fig. 3). Argentinian late Paleozoic–Triassic batholiths are also shown (4, Gregori and Benedini (2013); 5, SEGEMAR (2012)).

demonstrating a continuous magmatic evolution from the latest early Carboniferous to latest Triassic with a noticeable change in the middle Permian.

2. Materials and methods

The studied zircon grains are from 5 rock samples belonging to the Montosa–El Potro Batholith (28° to 28°30′S), which is part of the Chilean Frontal Andes (Fig. 1). Zircon grains were separated from 2 kg whole rock samples using standard techniques: grinding, Gemini table, heavy liquids and Frantz separation followed by final hand picking under a binocular microscope. Separating work was undertaken in the mineral separating facility of the Geology Department, University of Chile.

U–Th–Pb analyses were undertaken using a sensitive high-resolution ion microprobe (SHRIMP II) for defining the $^{206}Pb/^{238}U$ ages following standard procedures (Williams, 1998). Between 15 and 17 grains were analyzed in each sample to characterize the age variation present. Weighted mean $^{206}Pb/^{238}U$ ages were calculated and the uncertainties are reports as 95% confidence limits.

$\delta^{18}O$ analyses were carried out using a sensitive high resolution ion microprobe (SHRIMP SI) and electron gun for charge compensation (Ickert et al., 2008) in the exact same spots were the U–Pb analyses were obtained with SHRIMP II. Calculated $\delta^{18}O$ values were normalized relative to an FC1 weighted mean $\delta^{18}O$ value of +5.61‰.

Lu–Hf analyses were completed using laser ablation multi-collector inductively coupled plasma mass spectrometry (Neptune LA-MC-ICPMS) coupled with a HelEx 193 nm ArF Excimer laser ablation system (Eggins et al., 2005). Laser ablation analyses were done on the spots previously used for U–Pb and oxygen isotopes.

U–Pb, oxygen and Lu–Hf analytical labwork was undertaken at the Research School of Earth Sciences of the Australian National University in Canberra, Australia. Detailed analytical methods are found in Supplementary information.

3. Results and discussion

3.1. Chilean Frontal Andes (28°–28°30′S) results

Isotopic and geochronological analyses are summarized in Table 1. Full geochronological and isotopic data are provided in Supplementary data.

U–Pb zircon age determinations are summarized as follows (Fig. 2): La Estancilla pluton sample (IC-17) yielded a weighted mean $^{206}Pb/^{238}U$ age of 286 ± 2 Ma (MSWD = 1.17); Montosa sample (IC-22), 253 ± 2 Ma (MSWD = 0.81); El León sample (IC-58), 257 ± 2 Ma (MSWD = 0.97); Chollay sample (IC-91), 259 ± 2 Ma (MSWD = 0.94); and El Colorado sample (IC-93), 248 ± 2 Ma (MSWD = 1.17). Accordingly, La Estancilla pluton corresponds to Artinskian (early Permian) whilst the other 4 samples are very close to the Permian–Triassic boundary. All obtained ages can be confidently interpreted as igneous crystallization ages.

εHf_i values among the 5 units are generally overlapping (La Estancilla pluton: between −3.8 and +1.2; Montosa: between −3.2 and +1.6; El León: between −2.5 and +2.0; Chollay: between −1.3 and +2.8), with only one sample showing more positive values (El Colorado: between −2.7 and +4.7). There is not a noticeable variation within the εHf_i signatures among the units (most values range approximately from −3.0 to +3.0). On the other hand, La Estancilla pluton shows noticeable higher $\delta^{18}O$ values (approximately over 6.5‰, with $\delta^{18}O$ ranging from 6.6‰ to 7.5‰) compared to the other units (mainly below 6.5‰, with $\delta^{18}O$ ranging from 5.5‰ to 6.7‰ for Montosa; from 5.5‰ to 6.4‰ for El León; from 4.8‰ to 6.4‰ for Chollay; and from 4.4‰ to 6.0‰ for El Colorado).

Calculated two-stage Depleted Mantle model ages (T_{DM2}) range from 1.1 to 1.5 Ga (Mesoproterozoic) for La Estancilla pluton; from 1.1 to 1.4 Ga (Mesoproterozoic) for Montosa; from 1.1 to 1.3 Ga (Mesoproterozoic) for El León; from 1.0 to 1.3 Ga (Mesoproterozoic) for Chollay; and from 0.9 to 1.4 Ga (early Neoproterozoic–Mesoproterozoic) for El Colorado. These ages show a significant crustal residence time with inferred separation from a depleted mantle source during Mesoproterozoic times.

The 5 granitoid samples corresponding to a north-to-south distance along the Montosa–El Potro Batholith of ca. 50 km record a range in crystallization ages between 286 Ma and 248 Ma (early Permian to early Triassic). Isotopic εHf_i values do not show a considerable difference among the samples and range from −3.8 to +4.7, whereas $\delta^{18}O$ indicates a considerable difference between the oldest sample (IC-17) and the rest of them (IC-22, IC-58, IC-91 and IC-93): values range between 6.6‰ and 7.5‰ and 4.4‰ and 6.7‰ respectively. The new data largely fill a previous apparent 'gap' in the trend of Fig. 3 (between the Coastal Batholith and the Frontal Andes Batholith) making it now continuous from latest early Carboniferous to Triassic.

3.2. Hf–O isotopic signatures and U–Pb geochronological interpretations

Results indicate a clear and continuous trend from high values of $\delta^{18}O$ to mantle-like signatures with lower $\delta^{18}O$, as the rocks get younger (from ca. 9.3‰ during latest early Carboniferous to ca. 4.4‰ and lower in the late Triassic, Fig. 3). Despite its continuity, it is possible to separate units with or without 'mantle zircon values' at ca. 270 Ma (middle Permian). High values of $\delta^{18}O$ ($\delta^{18}O > 6.5$‰) indicate a continental crustal to supracrustal component (Taylor and Sheppard, 1986; Pietranik et al., 2013), and low εHf_i ($\varepsilon Hf_i < 0$), the addition of non-radiogenic continental crust-like material (Kemp et al., 2007). This isotopic signature is observed in both the Frontal Andes and the Coastal Range, with zircon isotope values of different samples completely superimposed (Fig. 3). This allows us to distinguish a stage from at least 325 Ma to 270 Ma (late Mississippian–middle Permian) in which magmas formed with a crustal component, and one from 270 Ma to 210 Ma (middle Permian–late Triassic) in which the magmas are dominated by mantle components. Another important feature is the fact that two-stage Depleted Mantle model age (T_{DM2}) calculations yielded Mesoproterozoic ages for all these samples, indicating that a component

Table 1
Summarized U–Pb SHRIMP II in zircon ages, initial εHf_i and $\delta^{18}O$ values for zircon spots from Montosa–El Potro Batholith.

Sample/unit	Geographical coordinates	Lithology	$^{206}Pb/^{238}U$ age (Ma)	Initial εHf_i	$\delta^{18}O$ (‰) (range/average)	T_{DM2} Hf (Ga)
IC-17/La Estancilla pluton	28°00′14″S 69°53′05″W	Hbl-bt tonalite	286 ± 2	−3.8 to +1.2	6.6–7.5/6.9	1.1–1.5
IC-22/Montosa	28°05′34″S 69°50′57″W	Hbl-bt tonalite	253 ± 2	−3.2 to +1.6	5.5–6.7/6.1	1.1–1.4
IC-58/El León	28°01′06″S 69°32′19″W	Bt-hbl monzogranite	257 ± 2	−2.5 to +2.0	5.5–6.4/6.1	1.1–1.3
IC-91/Chollay	28°28′17″S 69°43′25″W	Bt-hbl syenogranite	259 ± 2	−1.3 to +2.8	4.8–6.4/5.5	1.0–1.3
IC-93/El Colorado	28°24′38″S 69°47′11″W	Bt syenogranite	248 ± 2	−2.7 to +4.7	4.4–6.0/5.3	0.9–1.4

Note: T_{DM2}: two-stage Depleted Mantle model age.

of the magmas from which the zircons crystallized had a significant residence time and therefore the magmatic arc formed on continental crust. Part or all of the continental crust-like material required for the high $\delta^{18}O$ values could correspond to sediments transported deep into the mantle wedge by the subducting slab (Gerya and Meilick, 2011) or the isotopic signature could have been acquired through crustal contamination as the plutons were emplaced in the upper parts of the continental crust. Thus, the O–Hf compositions indicate a deep source of magmas, either affected by assimilation processes during magma ascent or with the influence of material acquired at depth, in the subcontinental mantle wedge.

The younger rocks of this study (<270 Ma) show markedly different $\delta^{18}O$ compositions to the rocks described above. They show $\delta^{18}O < 6.5‰$ (Fig. 3), along with a wider range of εHf_i values (mostly from −3 to +3). The $\delta^{18}O$ data (4.9 to 6.5‰) indicate mantle source magmas from which the zircons crystallized with no ingestion of continental crust or supracrustal material (units fall completely within the mantle zircon range; taken from Valley et al. (1998)) or minor participation of the latter ($\delta^{18}O$ slightly above the mantle zircon limit). In the case of εHf_i values, although they are very concordant, they show a tendency from less to more radiogenic as the rocks get younger. Positive εHf_i values indicate a more mantle-derived influence (Valley et al., 1998; Pietranik et al., 2013) (Fig. 3), which could reflect the addition of juvenile material in a foreland region (Dahlquist et al., 2013). Nevertheless, the overlap of isotopic data and ages does not allow a more specific differentiation among these samples and thus the differences can be attributed to variations in the magma source and/or in the magmatic differentiation processes. On the other hand, low $\delta^{18}O$ values (between 3.5 and 5.5‰) with positive εHf_i ratios (ca. +3 to +7) could be related to a subcontinental mantle source of magmas with assimilation of high temperature altered continental rocks or oceanic crust (Bindeman and Valley, 2001; Monani and Valley, 2001; Bolhar et al., 2008).

Some zircons, although showing mantle-like $\delta^{18}O$ values and εHf_i between +2 and −2, are from highly differentiated rocks (i.e. granites). This signature is normally a characteristic of mafic igneous rocks and can be observed in arc magmas contaminated by sediments, since the O-isotope signature is relatively insensitive to mixing with arc-subducted sediments (Nebel et al., 2011). Melting of old mafic crust, even with limited proportions of sediments, can produce mantle-like $\delta^{18}O$ signatures without a real involvement of mantle material (Clemens et al., 2011; Villaros et al., 2012; Pietranik et al., 2013). This means that the rocks emplaced during the middle Permian–Triassic could have involved melting of an old, thinned, mafic crust (e.g., IC-93, IC-91, Fig. 3) with more or less continental crust material involvement (e.g., IC-22, IC-58, Fig. 3). The newly formed magmas inherited mantle-like $\delta^{18}O$ values from the mafic crust (lower continental crust) and some of them were slightly contaminated with a continental crust component. The resulting rocks were more differentiated but preserved mantle-like $\delta^{18}O$ signatures. It can be postulated that this occurred in a thinned continental crust context — possibly due to an extensional setting.

Higher $\delta^{18}O$ samples could have resulted from subduction-related magmatism in a normal-to-thickened continental crust, with involvement of continental crust to supracrustal material. Such a tectonic setting has been proposed for the Coastal Batholith (Deckart et al., 2014), which in consequence could define a single magmatic belt together with the Frontal Cordillera batholiths. U–Pb zircon ages from previous works (e.g., Maksaev et al., 2014) (Fig. 1) allow us to identify continuous plutonism from 328 to 300 Ma along the entire belt between 21°S and 40°S. There was protracted plutonism from 328 to ca. 270 Ma north of 33°S in Chile, but subduction-related granitoids younger than 300 Ma are absent to the south. Furthermore, a single inherited zircon core from a 257 Ma sample (at around 28°S with mantle-like $\delta^{18}O$) yielded ca. 336 Ma and $\delta^{18}O$ and εHf_i values of 8.76‰ and −2.88 respectively, showing the same isotopic signatures as the rocks from the older units here analyzed. Despite that it may be arguable that it is only one zircon core, it still shows the same isotopic composition as the coeval zircon grains and therefore, it can give a glimpse of older rocks forming under the same tectonic conditions.

Although previous work (Charrier et al., 2014; Hervé et al., 2014) defined four magmatic groups ranging from latest early Carboniferous to late Triassic based on age clusters, their geochemical and isotopic characteristics are coherent with the two groups described here and also coincide with major episodes of volcanism (Maksaev et al., 2014). Rocks younger than middle Permian (<270 Ma) show a more juvenile isotopic composition whereas the older ones (i.e. latest early Carboniferous–early Permian), represent rocks syntectonically emplaced into thickened crust.

3.3. Magma genesis and geodynamic evolution

3.3.1. Pre–middle Permian

The Andean margin of Gondwana can be considered as an accretionary orogeny (Vaughan and Pankhurst, 2008). Between Silurian and Devonian periods, the Chilenia terrane accreted onto the western Pacific margin of Gondwana (Ramos et al., 1986; Bahlburg and Hervé, 1997) (Fig. 4A). Convergence in this segment may have started between ca. 343 and 310 Ma (Willner et al., 2012). Orogenic deformation due to changes in the intensity of plate convergence during that period marks the commencement of a major subduction cycle (Ramos and Alemán, 2000). Subsequently, from latest early Carboniferous to earliest middle Permian, high $\delta^{18}O$ isotopic signature plutons were emplaced in a subduction-related compressional setting, possibly as the roots of the magmatic arc beneath the Chilenia basement (Fig. 4B). This orogenic deformation corresponds to the Gondwanide Orogeny, which is also part of the end of the Terra Australis Orogen, starting with Rodinia break-up at ca. 630–530 Ma (Cawood, 2005). It includes the San Rafael event (ca. 284 Ma to 276 Ma), a compressional episode marked by intense folding and thrusting (Llambias and Sato, 1990) observed in the Argentinian Frontal Cordillera. In this tectonic configuration, isotopic data suggest a crustal to supracrustal component in the magmas and/or the influence of mature sediments transported through the subducted slab, given the increased $\delta^{18}O$ values and negative εHf_i, the latter indicating the input of less radiogenic, continental-like material.

This orogenic event was the result of a major global plate reorganization: the assembly of Pangea (Cawood, 2005), which occurred between ca. 320 and 280 Ma (Li and Powell, 2001) and was contemporaneous with the high $\delta^{18}O$ magmatism described above. In other words, all the magmatism from latest early Carboniferous to earliest middle Permian was emplaced in a subduction setting under orogenic conditions during the Gondwanide Orogeny as a consequence of the subduction of the Pantalassa Oceanic Plate under the southwestern margin of the assembling Pangea (Fig. 4B).

3.3.2. Post–middle Permian

After ca. 270 Ma and once Pangea was fully assembled, a new post-orogenic extensional setting was configured. Due to Pangea being in a static reference mode (Vilas and Valencio, 1978) or with arrested continental drift (Charrier et al., 2014) and in consequence, with ceasing or very low subduction velocities (Charrier et al., 2014), a new geodynamic scenario was configured. A low subducting plate velocity promotes a relatively steady hinge retreat (Schellart, 2005) resulting in backarc extension. Additionally, a plate rollback velocity greater than the movement of the continent towards the trench – which in the case of Pangea can be considered arrested – can also trigger backarc extension (Grocott and Taylor, 2002). This tectonic setting can be seen in two active continental margins today: East Asia and the Mediterranean (Schellart, 2005). Generalized extension at the southwestern margin of Pangea affected pre-existing zones of weakness (Charrier et al., 2014), particularly the hanging walls of sutures between the Paleozoic accreted terranes (Mpodozis and Ramos, 2008; Ramos, 2009). This resulted in the development of several NW–SE basins whose deposits

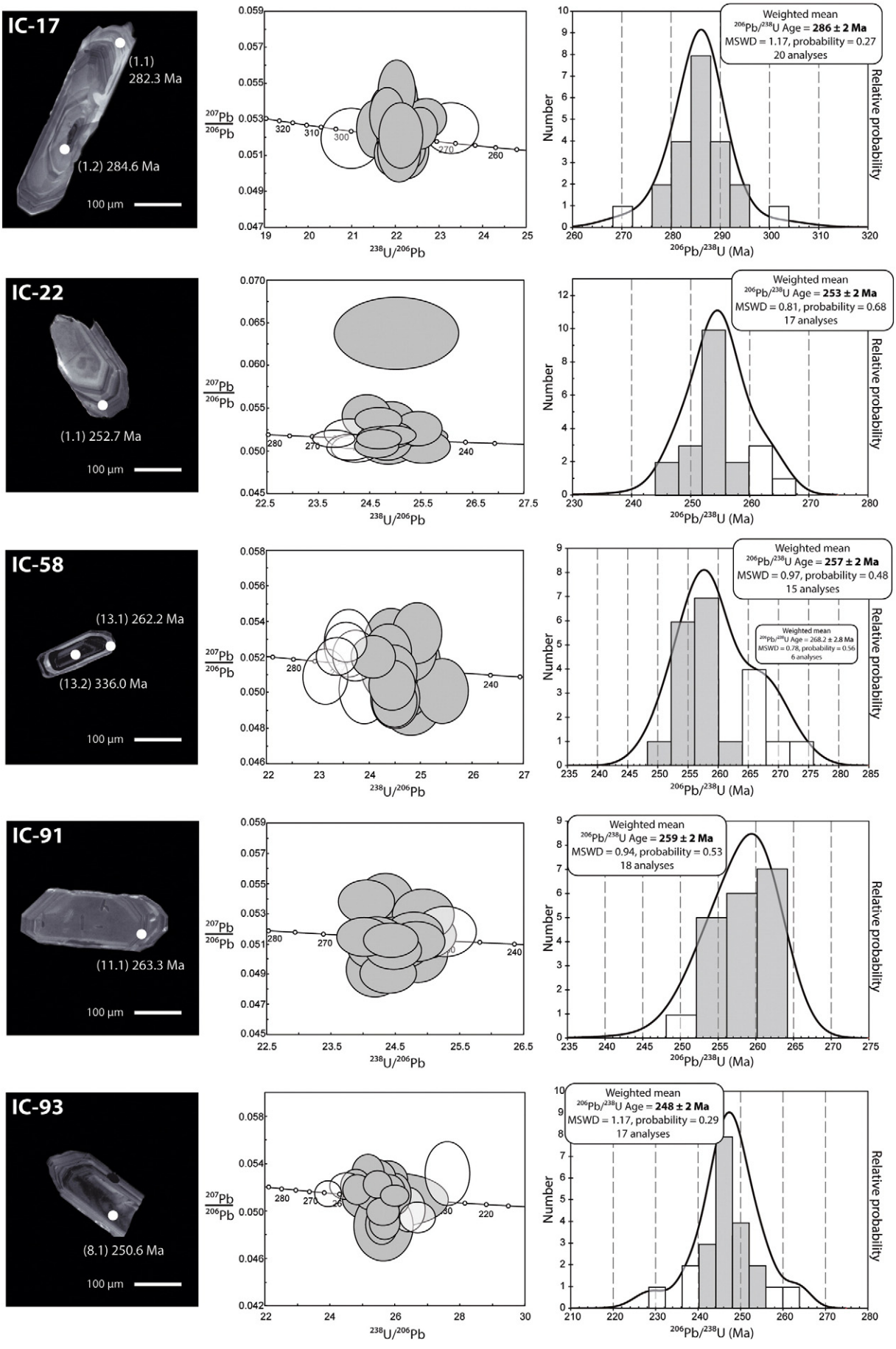
IC-17
(1.1)
282.3 Ma
(1.2) 284.6 Ma
100 µm
207Pb/206Pb
238U/206Pb
Weighted mean
206Pb/238U Age = 286 ± 2 Ma
MSWD = 1.17, probability = 0.27
20 analyses
Number
Relative probability
206Pb/238U (Ma)
IC-22
(1.1) 252.7 Ma
100 µm
Weighted mean
206Pb/238U Age = 253 ± 2 Ma
MSWD = 0.81, probability = 0.68
17 analyses
IC-58
(13.1) 262.2 Ma
(13.2) 336.0 Ma
100 µm
Weighted mean
206Pb/238U Age = 257 ± 2 Ma
MSWD = 0.97, probability = 0.48
15 analyses
Weighted mean
206Pb/238U Age = 268.2 ± 2.8 Ma
MSWD = 0.78, probability = 0.56
6 analyses
IC-91
(11.1) 263.3 Ma
100 µm
Weighted mean
206Pb/238U Age = 259 ± 2 Ma
MSWD = 0.94, probability = 0.53
18 analyses
IC-93
(8.1) 250.6 Ma
100 µm
Weighted mean
206Pb/238U Age = 248 ± 2 Ma
MSWD = 1.17, probability = 0.29
17 analyses

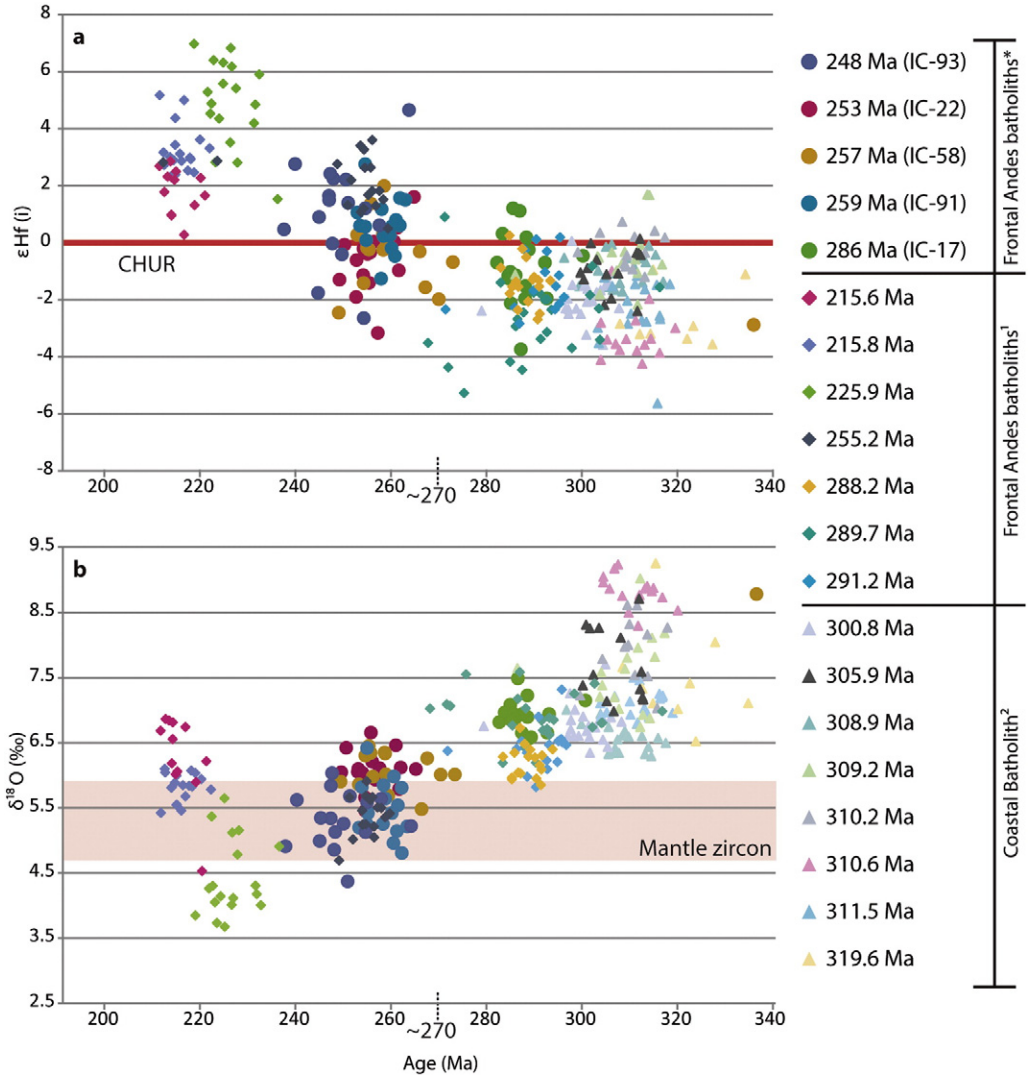

Fig. 3. Progressive isotopic evolution. a Initial εHf_i vs age (Ma) diagram; b, $\delta^{18}O$ vs age (Ma) diagram for the samples from the Chilean Frontal Andes (*this work); its continuation (1, Hervé et al. (2014)); and the Coastal Batholith (2, Deckart et al. (2014)). Samples extend from 20°S to 40°S. A clear and continuous trend in the magmatism from high values of $\delta^{18}O$ to mantle-like signatures can be seen. At ca. 270 Ma (middle Permian), isotopic signatures (especially with $\delta^{18}O$) indicate the evolution from continent-derived characteristics to mantle-like signatures revealing variations in the tectonic setting (see Section 3.2). Mantle zircon $\delta^{18}O$ range is taken from Valley et al. (1998).

are generally marine to continental from the coast to their inland prolongations (Charrier et al., 2014), including the rift-related bimodal sequences of the Choiyoi province (Kay et al., 1989). Moreover, considering at around 40°S the southernmost limit of the accreted Chilenia terrane (Ramos, 2009) and thus the area of the lateral slab edge, rapid rollback can be expected there (Schellart et al., 2007; Schellart, 2008). This results in significant upper plate extension within 1800 km of the lateral slab edge (Schellart et al., 2007) that can explain the increasing extensional-related magmatism and depocentres of the Triassic-earliest Jurassic rift systems towards 40°S (between 22° and 40°S ≈ 2000 km).

Slab rollback extension promoted the conditions for the mantle-like $\delta^{18}O$ and progressively higher εHf_i magmatism. As the continental crust thinned (orogenic collapse), decompression triggered melting in the mantle. Large amounts of juvenile basaltic magmas accumulated below the continental crust (underplating) providing sufficient heat for melting of the old thinned mafic crust and thus, new melts inherited mantle-like $\delta^{18}O$ signatures but relatively low εHf_i. This configuration lasted at least from 270 Ma to 210 Ma according to $\delta^{18}O$ and εHf_i signatures (Fig. 4C). However, the presence of bimodal magmatism (from 20°S to 31°S) until the late Triassic (ca. 205 Ma (Maksaev et al., 2014)) suggests that the slab rollback extensional setting was continuous throughout middle Permian and Triassic times. This scenario is coherent with slab rollback during early Carboniferous in the Eastern Sierras Pampeanas, Argentina (Alasino et al., 2012), thus making it a relatively continuous process (except for the San Rafael compressional event) which progressed westwards to the Chilean Frontal Andes, and ultimately defined the tectonic configuration during middle Permian–Triassic. εHf_i values reported here are within the range of previous results (Dahlquist et al., 2013, 2016), supporting the idea of addition of variable amounts of juvenile material in a foreland extensional region.

South of 31°S, progressive slab shallowing from ca. 300 to 290 Ma displaced the magmatism eastwards. Permian–Triassic plutonism was not developed in the Chilean margin but is present in Argentina. The shallower slab setting was not uniform from 31°S to 40°S; it was gradually shallower from 31°S to 36°S, completely flat between 36°S and 39°S and again shallower from 39°S to 40°S (Kleiman and Japas, 2009)

Fig. 2. Geochronological analyses. Cathodoluminescence images of representative zircon grains along Tera–Wasserburg concordia and age probability density plots (95% confidence limits) for each sample. IC-17: La Estancilla pluton; IC-22: Montosa; IC-58: El León; IC-91: Chollay; and IC-93: El Colorado.

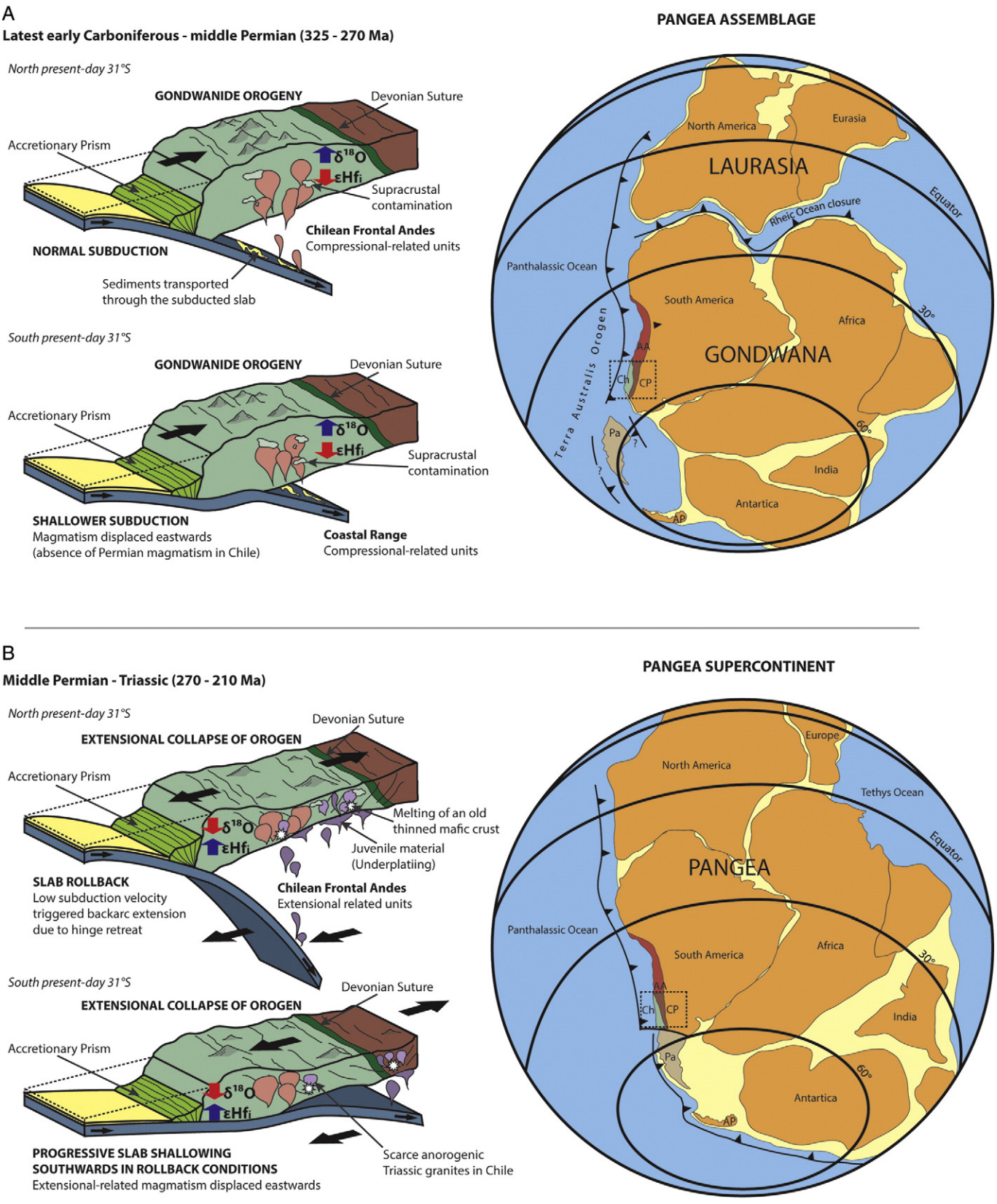

Fig. 4. Tectonic model. A. Latest early Carboniferous to earliest middle Permian: low values of εHf_i (ca. +1 to −4) with high $\delta^{18}O$ (ca. >6.5‰) indicate an elevated supracrustal component and the addition of less radiogenic continental-like material; magmas formed in a subduction-related continental arc during the Gondwanide Orogeny. B. Middle Permian to Triassic: a wider range of εHf_i values (ca. +3 to −3) with relatively low, mantle-like $\delta^{18}O$ (ca. 4.0–6.5‰) indicate magmas inheriting lower $\delta^{18}O$ values from the melting of an old thinned mafic crust. The higher positive values of εHf_i can be related to the influence of new juvenile material in the source of some magma; magmas formed in a slab rollback extensional setting. AA, Arequipa–Antofalla; CP, Cuyania–Precordillera; Ch, Chilenia; Pa, Patagonia; AP, the Antartic Peninsula. Global reconstruction based on previous work (Keppie and Ramos, 1999; Torsvik and Cocks, 2013).

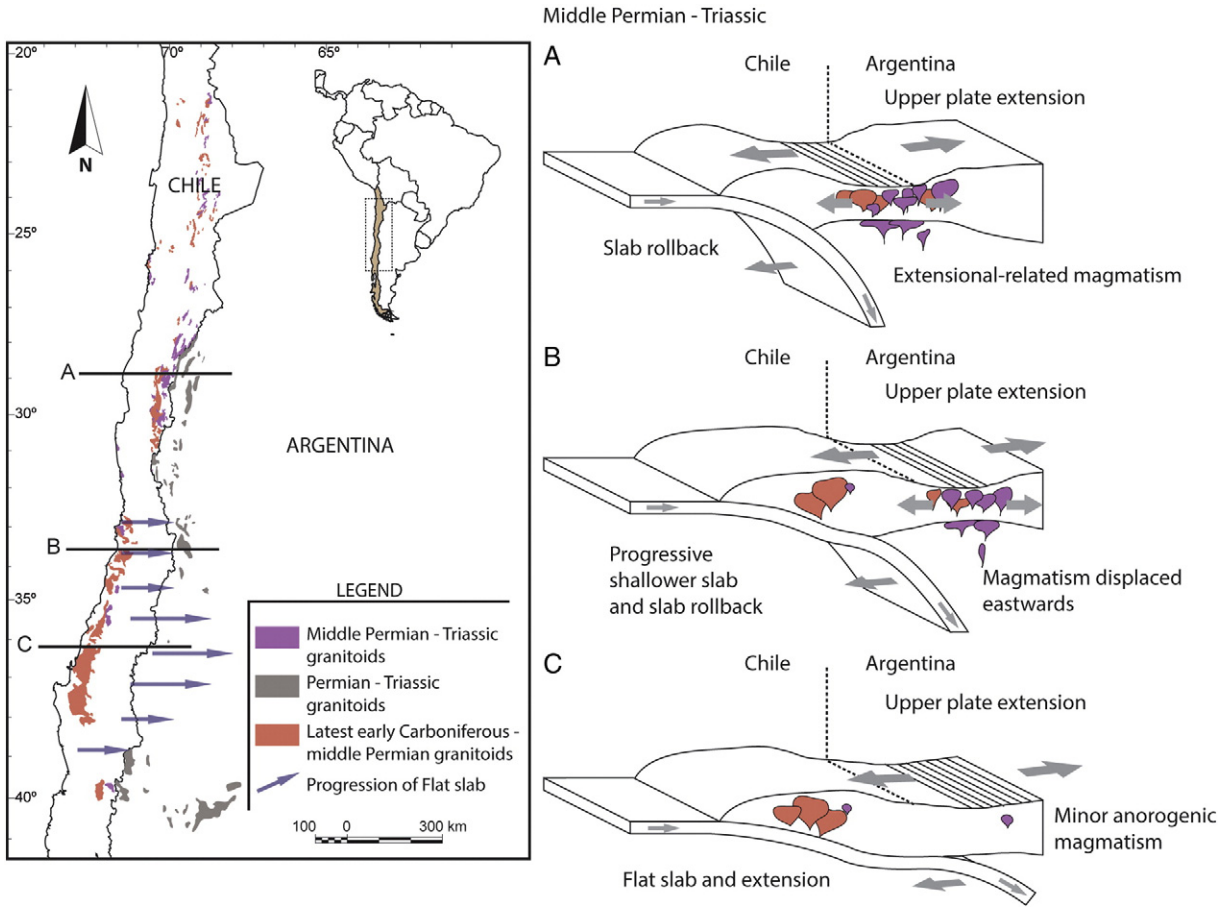

Fig. 5. Permian–Triassic flat slab evolution. The displacement of the Permian–Triassic magmatism eastwards south of 31°S can be explained by progressive slab shallowing and final flat-slab segmentation. It became gradually shallower from 31°S to 36°S, completely flat between 36°S and 39°S and again shallower from 39°S to 40°S. Section A shows extension-related magmatism without slab shallowing. Section B, progressively shallower slab (southward) shifted magmatism eastward (to Argentina). Section C shows the complete flat slab segment and low magmatic activity. Post-orogenic granitoids in the flat slab section can be attributed to crustal melting due to orogenic collapse (decompression) during the extensional period (middle Permian–Triassic). In sections: orange units represent latest early Carboniferous–middle Permian subduction-related magmatism; purple units, slab rollback middle Permian–Triassic extensional-related magmatism. Permian–Triassic units in Argentina (SEGEMAR, 2012; Gregori and Benedini, 2013) (gray on map) correspond to both subduction- and extension-related magmatism, in agreement with the timing of the tectonic evolution proposed here.

(Fig. 5). This segmentation explains the presence of subduction-related magmatism (ca. 276 Ma), which later changed into a transitional, post-orogenic crust-derived middle Permian (273–262 Ma) to Triassic bimodal magmatism in Argentina (Gregori and Benedini, 2013) (Fig. 5), in agreement with the isotopic interpretations presented here. Notwithstanding a shallower oceanic plate, arrested continental drift and slow subduction velocity prevailed. Thus, slab rollback extension was still present south of 31°S during middle Permian–Triassic times. In addition, scarce late Triassic anorogenic extensional-related A-type granites within the Coastal Batholith Range (Vásquez and Franz, 2008) can be linked to this tectonic setting as magmatism produced by crustal melting due to orogenic collapse. The results indicate a common setting for all the middle Permian–late Triassic magmatism from 20°S to 40°S: post-orogenic backarc extensional conditions due to slab rollback.

3.3.3. Overall geodynamic evolution

The latest early Carboniferous–middle Permian high $\delta^{18}O$ granitoids, as well as the middle Permian–Triassic extension-related plutonic complexes, formed a continuous magmatic belt at least between 20°S and 40°S. The magmatism progressively and almost uninterruptedly evolved from a continental-derived source towards mantle-like signatures from latest early Carboniferous to late Triassic as a response to the tectonic changes before, during and after Pangea Assembly (Fig. 4). First, subduction of the paleo-Pacific oceanic plate (Panthalassa Ocean) under the western margin of paleo-South America (southwestern margin of Gondwana) was the cause of the crust-derived magmatism, which was syntectonic with compressional deformation of the San Rafael Tectonic Event during the Gondwanide Orogeny. Subsequently, and throughout the existence of Pangea as a supercontinent (after ca. 270 Ma), low subduction velocity triggered steady backarc extension and related magmatism due to hinge retreat. Progressive slab shallowing from 31°S southward (starting ca. 300–290 Ma), shifted magmatism inland. This tectonic configuration remained continuous until the latest Triassic, when the initial break-up of the Pangea Supercontinent took place (ca. 200 Ma (Deckart et al., 1998; Veevers, 2005; Torsvik and Cocks, 2013)). Changes of the plate dynamics from the static mode of Pangea towards an increased convergence rate of the newly re-established Gondwana (with higher subduction velocity) concluded slab rollback extension and thus, its magmatism in the backarc region. Because of the new conditions, and possibly in association with steepening of the oceanic subducting plate, magmatism was displaced westwards (i.e. trenchward), occurring primarily within the mantle wedge overlying the subducted slab (Pankhurst et al., 1988). This tectonic evolution is coherent with the presence of the early–late Jurassic magmatic arc in the Coastal Range (Charrier et al., 2014), stretching from southern Peru to central Chile (Mpodozis and Ramos, 2008). The locus of plutonism jumped to the Coastal Range from the east by the beginning of the Jurassic in an almost non-magmatic episode (scarce presence of latest Triassic–earliest Jurassic plutons: ca. 205–200 Ma), which is comparable to the jump of the magmatism from the Coastal Range to the High Andes (west to

east) during Cenozoic times (Parada et al., 2007). The magmatism (between 195 and 155 Ma) occurred in an extensional intra-arc basin due to sinistral movement in a high-stress regime with oblique convergence (Parada et al., 2007).

Finally, the continuous north to south latest early Carboniferous–Triassic magmatic belt was displaced from east to west by Mesozoic extension and basin development (Parada et al., 2007), while the corresponding South American continent was essentially static in a mantle reference framework (Brown, 1991). The displacement of the magmatic belt can be seen at ca. 31°–32°S (Fig. 1), corresponding to the Coastal Batholith and the Frontal Andes batholiths, as well as by the occurrence of late Paleozoic–Triassic plutonic rocks in the Coastal Range and Frontal Andes at 26°S (Brown, 1991) (Fig. 1).

4. Conclusions

We propose that tectonic conditions from the latest early Carboniferous to late Triassic and the continuity of magmatism, strongly supported by the geological records, are the results of the subduction-related convergent evolution of the paleo-Pacific border of Pangea since the Terra Australis Orogen until its break-up (i.e. 200 Ma (Deckart et al., 1998), among others). Furthermore, the progressive evolution from an orogenic compressional setting with expansion of magmatism to later slab shallowing (with flat slab in the southern region), extension, orogenic collapse and slab steepening, allows us to re-define the Andean orogenic cycle (at least between latitudes 20°S and 40°S), as a continuous subduction-related process since the latest early Carboniferous to the present day. Consequently, its roots are linked to the Terra Australis Orogen. The sequence of events is in agreement with the idealized tectonic evolution of an Andean orogenic cycle (Ramos, 2009) where the angle of subduction is the key factor controlling magma-mixing processes (Pankhurst et al., 1988). In addition to that, the expected westward retreat of the arc at the beginning of the Jurassic due to the end of slab rollback also fits the idealized model. There is no reason to consider cessation of subduction during the late Permian/Triassic and its renovation in the early Jurassic (Mpodozis and Kay, 1992; Franzese and Spalletti, 2001), and therefore the existence of the hypothetic 'terrane X' (Mpodozis and Kay, 1992). The Andean orogenic cycle due to the subduction of the Pacific/paleo-Pacific oceanic plate underneath South America/paleo-South America has been a continuous process since the late Paleozoic. The major differences observed since that period are the prevailing global geodynamic conditions. While Pangea was being assembled, those conditions were different enough (compared to the traditionally defined Andean orogenic cycle; e.g. Charrier et al. (2014)) to produce noticeable changes in the magmatism (i.e. extreme extensional conditions due to low subducting plate velocities and slab rollback). Analogue models (Schellart, 2008) demonstrate that low subduction velocities trigger backarc extension due to hinge retreat. Also, Jurassic intrusions are located in a belt from 20°S to 36°S, ending at the beginning of the flat-slab segment (also present in the eastern margin of the Southern Patagonian batholith south of 48°S; Hervé et al. (2007)). The Paleozoic accretionary history of the south-western margin of Gondwana (up to 40°S) was completely finished by latest early Carboniferous and was followed by the Andean subduction, a continuous process since Paleozoic times and not from the early Jurassic as previously thought (e.g. Mpodozis and Kay, 1992; Charrier et al., 2014). Distinctive magmatism during the mid Permian–Triassic was due to Pangea Assembly, a unique and global event that conditioned geodynamic processes worldwide. Moreover, the presence of a rift-related belt of magmatism in Peru and Bolivia from the late Permian–middle Jurassic (Sempere et al., 2002) allows us to speculate the idea of the continuity of the Andean orogenic cycle northward to 8°S–20°S. Nevertheless, more evidence is required to confirm this hypothesis. The new tectonic model proposed here, unravels the paradigm of the latest early Carboniferous–Triassic magmatism in Chile and provides an argument for an uninterrupted convergent plate margin setting for the vast late Paleozoic–early Mesozoic magmatism in Chile and Argentina. This model also shows how global geodynamics (i.e. assemblage and break-up of supercontinents) are a key factor in the occurrence of certain type of magmatism (rifting-related A-type granites; e.g., Mpodozis and Kay (1992)) which otherwise can be considered 'odd' if analyzed only from a local point of view.

Acknowledgements

We thank Juan Vargas and Roberto Valles (Universidad de Chile) for the zircon separation; Dr. Mark Fanning (ANU) for the Lu–Hf, O and U–Pb analytical work at the ANU; and Drs. Jacobus Le Roux and Gregory De Pascale (Universidad de Chile) for the English language corrections. The authors would like to acknowledge the constructive comments and discussions by Dr. Robert Pankhurst during revision of the manuscript. This research was funded by the Servicio Nacional de Geología y Minería (SERNAGEOMIN) project Plan Nacional de Geología (Geological Map 'Iglesia Colorada — Cerro El Potro') and the Masters fellowship of the Comisión Nacional de Investigación Científica y Tecnológica — CONICYT (grant no. 221320626). Additional funding was provided by the Departamento de Postgrado y Postítulo, Universidad de Chile. This work is part of the M.Sc. thesis of the principal author.

Appendix A. Supplementary data

Supplementary data to this article can be found online at http://dx.doi.org/10.1016/j.gr.2016.06.008.

References

Alasino, P.H., Dahlquist, J.A., Pankhurst, R.J., Galindo, C., Casquet, C., Rapela, C.W., Larrovere, M.A., Fanning, C.M., 2012. Early Carboniferous sub- to mid-alkaline magmatism in the Eastern Sierras Pampeanas, NW Argentina: a record of crustal growth by the incorporation of mantle-derived material in an extensional setting. Gondwana Research 22, 992–1008. http://dx.doi.org/10.1016/j.gr.2011.12.011.

Álvarez, J., Mpodozis, C., Arriagada, C., Astini, R., Morata, D., Salazar, E., Valencia, V.A., Vervoort, J.D., 2011. Detrital zircons from late Paleozoic accretionary complexes in north-central Chile (28°–32°S): possible fingerprints of the Chilenia terrane. Journal of South American Earth Sciences 32, 460–476. http://dx.doi.org/10.1016/j.jsames.2011.06.002.

Bahlburg, H., Hervé, F., 1997. Geodynamic evolution and tectonostratigraphic terranes of northwestern Argentina and northern Chile. Geological Society of America Bulletin 109, 869–884. http://dx.doi.org/10.1130/0016-7606(1997)109<0869.

Bindeman, I.N., Valley, J.W., 2001. Low-delta O-18 rhyolites from Yellowstone: magmatic evolution based on analyses of zircons and individual phenocrysts. Journal of Petrology 42, 1491–1517. http://dx.doi.org/10.1093/petrology/42.8.1491.

Bolhar, R., Weaver, S.D., Whitehouse, M.J., Palin, J.M., Woodhead, J.D., Cole, J.W., 2008. Sources and evolution of arc magmas inferred from coupled O and Hf isotope systematics of plutonic zircons from the Cretaceous Separation Point Suite (New Zealand). Earth and Planetary Science Letters 268, 312–324. http://dx.doi.org/10.1016/j.epsl.2008.01.022.

Brown, M., 1991. Comparative geochemical interpretation of Permian–Triassic plutonic complexes of the Coastal Range and Altiplano (25°30′ to 26°30′S), northern Chile. Geological Society of America Special Papers 265.

Cawood, P.A., 2005. Terra Australis Orogen: Rodinia breakup and development of the Pacific and Iapetus margins of Gondwana during the Neoproterozoic and Paleozoic. Earth-Science Reviews 69, 249–279. http://dx.doi.org/10.1016/j.earscirev.2004.09.001.

Charrier, R., Ramos, V.A., Tapia, F., Sagripanti, L., 2014. Tectono-stratigraphic evolution of the Andean Orogen between 31° and 37° S (Chile and Western Argentina). Geological Society of London, Special Publication 399, 13–61. http://dx.doi.org/10.1144/SP399.20.

Clemens, J.D., Stevens, G., Farina, F., 2011. The enigmatic sources of I-type granites: the peritectic connexion. Lithos 126, 174–181. http://dx.doi.org/10.1016/j.lithos.2011.07.004.

Dahlquist, J.A., Pankhurst, R.J., Gaschnig, R.M., Rapela, C.W., Casquet, C., Alasino, P.H., Galindo, C., Baldo, E.G., 2013. Hf and Nd isotopes in Early Ordovician to Early Carboniferous granites as monitors of crustal growth in the Proto-Andean margin of Gondwana. Gondwana Research 23, 1617–1630. http://dx.doi.org/10.1016/j.gr.2012.08.013.

Dahlquist, J.A., Pankhurst, R.J., Rapela, C.W., Basei, M.A.S., Alasino, P.H., Saavedra, J., Baldo, E.G., Murra, J.A., da Costa Campos Neto, M., 2016. The Capilla del Monte pluton, Sierras de Córdoba, Argentina: the easternmost Early Carboniferous magmatism in the pre-Andean SW Gondwana margin. International Journal of Earth Sciences http://dx.doi.org/10.1007/s00531-015-1249-0.

Deckart, K., Féraud, G., Marques, L.S., Bertrand, H., 1998. New time constraints on dyke swarms related to the Paraná-Etendeka magmatic province, and subsequent South Atlantic opening, southeastern Brazil. Journal of Volcanology and Geothermal Research 80, 67–83. http://dx.doi.org/10.1016/S0377-0273(97)00038-3.

Deckart, K., Hervé, F., Fanning, M., Ramírez, V., Calderón, M., Godoy, 2014. U–Pb geochronology and Hf–O isotopes of zircons from the Pennsylvanian Coastal Batholith, South-Central Chile. Andean Geology 41, 49–82. http://dx.doi.org/10.5027/andgeoV41n1-a03.
Eggins, S.M., Grün, R., McCulloch, M.T., Pike, A.W.G., Chappel, J., Kinsley, L., Mortimer, G., Shelley, M., Murray-Wallace, C.V., Spötl, C., Taylor, L., 2005. In situ U-series dating by laser-ablation multi-collector ICPMS; new prospects for Quaternary geochronology. Quaternary Science Reviews 24, 2523–2538.
Franzese, J.R., Spalletti, L.a., 2001. Late Triassic–early Jurassic continental extension in southwestern Gondwana: tectonic segmentation and pre-break-up rifting. Journal of South American Earth Sciences 14, 257–270. http://dx.doi.org/10.1016/S0895-9811(01)00029-3.
Gerya, T.V., Meilick, F.I., 2011. Geodynamic regimes of subduction under an active margin: effects of rheological weakening by fluids and melts. Journal of Metamorphic Geology 29, 7–31. http://dx.doi.org/10.1111/j.1525-1314.2010.00904.x.
Gregori, D., Benedini, L., 2013. The Cordon del Portillo Permian magmatism, Mendoza, Argentina, plutonic and volcanic sequences at the western margin of Gondwana. Journal of South American Earth Sciences 42, 61–73. http://dx.doi.org/10.1016/j.jsames.2012.07.010.
Grocott, J., Taylor, G.K., 2002. Magmatic arc fault systems, deformation partitioning and emplacement of granitic complexes in the Coastal Cordillera, north Chilean Andes (25°30′S to 27°00′S). Journal of the Geological Society of London 159, 425–442. http://dx.doi.org/10.1144/0016-764901-124.
Hervé, F., Pankhurst, R.J., Fanning, C.M., Calderón, M., Yaxley, G.M., 2007. The South Patagonian batholith: 150 my of granite magmatism on a plate margin. Lithos 97, 373–394. http://dx.doi.org/10.1016/j.lithos.2007.01.007.
Hervé, F., Fanning, C.M., Calderón, M., Mpodozis, C., 2014. Early Permian to Late Triassic batholiths of the Chilean Frontal Cordillera (28°–31°S): SHRIMP U–Pb zircon ages and Lu–Hf and O isotope systematics. Lithos 184-187, 436–446. http://dx.doi.org/10.1016/j.lithos.2013.10.018.
Ickert, R.B., Hiess, J., Williams, I.S., Holden, P., Ireland, T.R., Lanc, P., Schram, N., Foster, J.J., Clement, S.W., 2008. Determining high precision, in situ, oxygen isotope ratios with a SHRIMP II: analyses of MPI-DING silicate-glass reference materials and zircon from contrasting granites. Chemical Geology 257, 114–128.
Kay, S.M., Ramos, V.A., Mpodozis, C., Sruoga, P., 1989. Late Paleozoic to Jurassic silicic magmatism at the Gondwana margin: analogy to the Middle Proterozoic in North America? Geological Society of America 17, 324–328. http://dx.doi.org/10.1130/0091-7613(1989)017<0324.
Kemp, A.I.S., Hawkesworth, C.J., Foster, G.L., Paterson, B.A., Woodhead, J.D., Hergt, J.M., Gray, C.M., Whitehouse, M.J., 2007. Magmatic and crustal differentiation history of granitic rocks from Hf–O isotopes in zircon. Science 315, 980–983. http://dx.doi.org/10.1126/science.1136154 (80-.).
Keppie, J.D., Ramos, V.A., 1999. Odyssey of terranes in the Iapetus and Rheic oceans during the Paleozoic. Geological Society of America 336, 267–276.
Kleiman, L.E., Japas, M.S., 2009. The Choiyoi volcanic province at 34°S–36°S (San Rafael, Mendoza, Argentina): implications for the Late Palaeozoic evolution of the southwestern margin of Gondwana. Tectonophysics 473, 283–299. http://dx.doi.org/10.1016/j.tecto.2009.02.046.
Li, Z.X., Powell, C.M., 2001. An outline of the palaeogeographic evolution of the Australasian region since the beginning of the Neoproterozoic. Earth-Science Reviews 53, 237–277. http://dx.doi.org/10.1016/S0012-8252(00)00021-0.
Llambias, E.J., Sato, A.M., 1990. El Batolito de Colangüil (29-31°S) Cordillera Frontal de Argentina: estructura y marco tectónico. Revista Geologica de Chile 17, 89–108.
Maksaev, V., Munizaga, F., Tassinari, C., 2014. Timing of the magmatism of the paleo-Pacific border of Gondwana: U–Pb geochronology of Late Paleozoic to Early Mesozoic igneous rocks of the north Chilean Andes between 20° and 31°S. Andean Geology 41, 447–506. http://dx.doi.org/10.5027/andgeoV41n3-a01.
Monani, S., Valley, J.W., 2001. Oxygen isotope ratios of zircon: magma genesis of low $\delta^{18}O$ granites from the British Tertiary igneous province, western Scotland. Earth and Planetary Science Letters 184, 377–392. http://dx.doi.org/10.1016/S0012-821X(00)00328-9.
Mpodozis, C., Kay, S.M., 1992. Late Paleozoic to Triassic evolution of the Gondwana margin: evidence from Chilean Frontal cordilleran batholiths (28°S to 31°S). Geological Society of America Bulletin 104, 999–1014. http://dx.doi.org/10.1130/0016-7606(1992)104<0999:LPTTEO>2.3.CO;2.
Mpodozis, C., Ramos, V.A., 2008. Tectónica jurásica en Argentina y Chile: extensión, subducción oblicua, rifting, deriva y colisiones? Revista de la Asociación Geológica Argentina 63, 481–497.
Nebel, O., Vroon, P.Z., van Westrenen, W., Iizuka, T., Davies, G.R., 2011. The effect of sediment recycling in subduction zones on the Hf isotope character of new arc crust, Banda arc, Indonesia. Earth and Planetary Science Letters 303, 240–250. http://dx.doi.org/10.1016/j.epsl.2010.12.053.
Pankhurst, R., Hole, M., Brook, M., 1988. Isotope evidence for the origin of Andean granites. Transactions of the Royal Society of Edinburgh: Earth Sciences 79, 123–133.
Parada, M.A., López-Escobar, L., Oliveros, V., Fuentes, F., Morata, D., Calderón, M., Aguirre, L., Féraud, G., Espinoza, F., Moreno, H., Figueroa, O., Muñoz Ravo, J., Troncoso Vásquez, R., Stern, C.R., 2007. Andean magmatism. In: Moreno, T., Gibson, W. (Eds.), The Geology of Chile. The Geological Society, London, pp. 115–146.
Pietranik, A., Słodczyk, E., Hawkesworth, C.J., Breitkreuz, C., Storey, C.D., Whitehouse, M., Milke, R., 2013. Heterogeneous zircon cargo in voluminous Late Paleozoic rhyolites: Hf, O isotope and Zr/Hf records of plutonic to volcanic magma evolution. Journal of Petrology 54, 1483–1501. http://dx.doi.org/10.1093/petrology/egt019.
Ramos, V.A., 1988. The tectonics of the Central Andes; 30° to 33°S latitude. Geological Society of America 31–54. http://dx.doi.org/10.1130/SPE218-p31.
Ramos, V.A., 2008. Patagonia: a Paleozoic continent adrift? Journal of South American Earth Sciences 26, 235–251. http://dx.doi.org/10.1016/j.jsames.2008.06.002.
Ramos, V.A., 2009. Anatomy and global context of the Andes: main geologic features and the Andean orogenic cycle. Memoir - Geological Society of America 204, 31–65. http://dx.doi.org/10.1130/2009.1204(02).
Ramos, V.A., Alemán, A., 2000. Tectonic evolution of the Andes. In: Cordani, E.U.J., Milani, E.J., Thomaz Filho, A., Campos, D.A. (Eds.), Tectonic Evolution of South America: Río de Janeiro, 31st International Geological Congress, pp. 635–685.
Ramos, V.A., Jordan, T.E., Allmendinger, R.W., Mpodozis, C., Kay, S.M., Cortés, J.M., Palma, M., 1986. Paleozoic terranes of the Central Argentine-Chilean Andes. Tectonics 5, 855–880. http://dx.doi.org/10.1029/TC005i006p00855.
Schellart, W.P., 2005. Influence of the subducting plate velocity on the geometry of the slab and migration of the subduction hinge. Earth and Planetary Science Letters 231, 197–219. http://dx.doi.org/10.1016/j.epsl.2004.12.019.
Schellart, W.P., 2008. Overriding plate shortening and extension above subduction zones: a parametric study to explain formation of the Andes Mountains. Bulletin Geological Society of America 120, 1441–1454. http://dx.doi.org/10.1130/B26360.1.
Schellart, W.P., Freeman, J., Stegman, D.R., Moresi, L., May, D., 2007. Evolution and diversity of subduction zones controlled by slab width. Nature 446, 308–311. http://dx.doi.org/10.1038/nature05615.
SEGEMAR, 2012. Sistema de Información Geográfica del Servicio Geológico Minero Argentino [WWW Document] (URL sig.segemar.gov.ar).
Sempere, T., Carlier, G., Soler, P., Fornari, M., Carlotto, V., Jacay, J., Arispe, O., Néraudeau, D., Cárdenas, J., Rosas, S., Jiménez, N., 2002. Late Permian–Middle Jurassic lithospheric thinning in Peru and Bolivia, and its bearing on Andean-age tectonics. Tectonophysics 345, 153–181. http://dx.doi.org/10.1016/S0040-1951(01)00211-6.
Taylor, H., Sheppard, S., 1986. Igneous rocks; I, Processes of isotopic fractionation and isotopic systematics. Reviews in Mineralogy and Geochemistry 16, 227–271.
Torsvik, T.H., Cocks, L.R.M., 2013. Gondwana from top to base in space and time. Gondwana Research 24, 999–1030. http://dx.doi.org/10.1016/j.gr.2013.06.012.
Valley, J.W., Kinny, P.D., Schulze, D.J., Spicuzza, M.J., 1998. Zircon megacrysts from kimberlite: oxygen isotope variability among mantle melts. Contributions to Mineralogy and Petrology 133, 1–11. http://dx.doi.org/10.1007/s004100050432.
Vásquez, P., Franz, G., 2008. The Triassic Cobquecura Pluton (Central Chile): an example of a fayalite-bearing A-type intrusive massif at a continental margin. Tectonophysics 459, 66–84. http://dx.doi.org/10.1016/j.tecto.2007.11.067.
Vaughan, A.P.M., Pankhurst, R.J., 2008. Tectonic overview of the West Gondwana margin. Gondwana Research 13, 150–162. http://dx.doi.org/10.1016/j.gr.2007.07.004.
Veevers, J.J., 2005. Edge tectonics (trench rollback, terrane export) of Gondwanaland-Pangea synchronized by supercontinental heat. Gondwana Research 8, 449–456. http://dx.doi.org/10.1016/S1342-937X(05)71147-3.
Vilas, J.F., Valencio, D.A., 1978. Paleomagnetism of South American and African rocks and the age of the South Atlantic. Revista Brasileira de Geociencias 8, 3–10.
Villaros, A., Buick, I.S., Stevens, G., 2012. Isotopic variations in S-type granites: an inheritance from a heterogeneous source? Contributions to Mineralogy and Petrology 163, 243–257. http://dx.doi.org/10.1007/s00410-011-0673-9.
Williams, I.S., 1998. U–Th–Pb geochronology by ion microprobe. In: McKibben, M.A., Shanks, W.C., Ridley, W.I. (Eds.), Reviews in Economic Geology, pp. 1–35.
Willner, A.P., Massone, H.-J., Ring, U., Sudo, M., Thomson, S.N., 2012. P–T evolution and timing of a late Palaeozoic fore-arc system and its heterogeneous Mesozoic overprint in north-central Chile (latitudes 31–32°S). Geological Magazine 149, 177–207. http://dx.doi.org/10.1017/S0016756811000641.